Mathematical Geology, Vol. 28, No. 1, 1996

Multifractal Modeling and Spatial Statistics[1]

Qiuming Cheng[2] and Frederik P. Agterberg[3]

In general, the multifractal model provides more information about measurements on spatial objects than a fractal model. It also results in mathematical equations for the covariance function and semivariogram in spatial statistics which are determined primarily by the second-order mass exponent. However, these equations can be approximated by power-law relations which are comparable directly to equations based on fractal modeling. The multifractal approach is used to describe the underlying spatial structure of De Wijs's example of zinc values from a sphalerite-bearing quartz vein near Pulacayo, Bolivia. It is shown that these data are multifractal instead of fractal, and that the second-order mass exponent (= 0.979 ± 0.011 for the example) can be used in spatial statistical analysis.

KEY WORDS: autocorrelation, fractals, mass exponents, multifractal spectrum, semivariogram, spatial covariance.

INTRODUCTION

The concept of multifractals has been developed and applied recently in physics and chemistry where this approach was shown to be useful for the study of the spatial distribution of physical and chemical quantities with geometrical support consisting of a set of points or spatial objects which may itself be fractal (Feder, 1988). In general, fractal sets can be measured by determining their presence or absence in collections of cells created by the partitioning of k-dimensional space $\mathbf{R}^k$ ($k = 1, 2,$ or 3). For multifractals, the amount of random variable is measured in the collections of cells.

Multifractals are spatially intertwined fractals with a continuous spectrum of fractal dimensions (cf. Stanley and Meakin, 1988; Evertsz and Mandelbrot, 1992; Agterberg, 1994). From the multifractal model various fractal models can be derived which may have different fractal dimensions including the box-counting, information, and correlation or cluster dimensions (Hentschel and Procaccia, 1983; Feder, 1988). In general, different fractal sets defined on complex

[1]Received 6 March 1995; accepted 16 June 1995.

[2]Ottawa-Carleton Geoscience Centre, University of Ottawa, Ottawa K1N 6N5, Canada.

[3]Geological Survey of Canada, 601 Booth Street, Ottawa K1A 0E8, Canada.

0882-8121/96/0100-0001$09.50/1

geometrical patterns with the property of self-similarity can be interrelated by means of multifractal theory.

In this paper, new results will be presented for the relationship between multifractal models and spatial statistics, consisting of autocorrelation, covariance, and semivariogram functions in spatial statistics. The usefulness of the new approach will be demonstrated by application to De Wijs's example of zinc values from a sphalerite-quartz vein near Pulacayo in Bolivia. This dataset was used previously to illustrate other, related geostatistical models (De Wijs, 1951; Matheron, 1962; Agterberg, 1994).

THE MULTIFRACTAL MODEL

Suppose $\mu(S_A)$ represents the measure of a set S in a segment A of $\mathbf{R}^k$. For the applications in this paper, $k = 1$. A line segment of length L can be partitioned into $N(\epsilon)$ cells (intervals) of equal size ϵ; let $\mu_i(\epsilon)$ denote the measure on S for the ith cell of size ϵ in $(0, L]$ with $i = 1, 2, \ldots, N(\epsilon)$. The partition function (Evertsz and Mandelbrot, 1992) is defined as

$$\chi_q(\epsilon) = \sum_{i=1}^{N(\epsilon)} \mu_i^q(\epsilon) \tag{1}$$

If the measure $\mu_i(\epsilon)$ satisfies the multifractal model, the partition function of Equation (1) has a power-law relation with cell size ϵ for any order q with $-\infty \leq q \leq \infty$, or

$$\chi_q(\epsilon) \propto \epsilon^{\tau(q)} \tag{2}$$

where $\propto$ represents proportionality, and $\tau(q)$ is the mass exponent of order q. Normally, only integer numbers are used for q but this is not required. From Equation (2), the singularity exponent $\alpha(q)$ and multifractal spectrum $f(\alpha) = f\{\alpha(q)\}$ can be obtained successively by

$$\alpha(q) = \frac{d\tau(q)}{dq}; \qquad f(\alpha) = q\alpha(q) - \tau(q) \tag{3}$$

The function $f(\alpha)$ can be interpreted as the negative of the Legendre transform of $\tau(q)$ (Evertsz and Mandelbrot, 1992). Each point along the curve for the spectrum $f(\alpha)$ represents the fractal dimension of a subset of S with approximately the same singularity exponent α. The maximum value $f_{\max}\{\alpha(0)\}$, which is reached for $q = 0$, corresponds to the box-counting fractal dimension. For a one-dimensional set, $f_{\max}\{\alpha(0)\} \leq 1$. The value $f\{\alpha(1)\}$ for $q = 1$ is the entropy dimension; $f\{\alpha(2)\}$ follows from $\alpha(2)$ and $\tau(2)$. The spatial correlation of continuous random variables and the clustering in point patterns are determined primarily by the second-order mass exponent $\tau(2)$.

Several multifractal spectra in physics and chemistry have the property $f_{\min}\{\alpha(\infty)\} = f_{\min}\{\alpha(-\infty)\} = 0$, although this is not a requirement. It may not be possible to establish this with certainty because $\tau(q)$ increasingly is determined only by the largest and smallest values of $\mu_i(\epsilon)$ as q tends to ∞ and $-\infty$, respectively. If $f_{\min}\{\alpha(\infty)\} = 0$, the largest values of $\mu_i(\epsilon)$ may satisfy a Pareto frequency distribution even when the lognormal distribution provides a first approximation for most other values (Mandelbrot and Evertsz, 1991; Agterberg, Cheng, and Wright, 1993; Cheng, Agterberg, and Ballantyne, 1994).

Multifractal theory was developed originally in the context of physics and chemistry. Recently, Evertsz and Mandelbrot (1992) have pointed out the analogy of Equation (1) with moment generating functions in statistical theory. Chernoff's theorem for large deviations (Billingsley, 1986, p. 147; Csörgö and Révész, 1981, p. 99) can be used to derive Equation (3).

Spatial random variables can have multifractal properties for any q with $-\infty \leq q \leq \infty$. A weaker assumption is that the multifractal model is valid only for $q = 1$ and 2. This assumption of second-order multifractality is sufficient to derive exact and approximate expressions for the covariance, autocorrelation, and semivariogram functions of continuous random variables in spatial statistics.

SPATIAL CORRELATION OF RANDOM VARIABLES IN R^1

Suppose that $X_i(\epsilon) = \epsilon^{-1}\mu_i(\epsilon)$, with $i = 1, \ldots, N(\epsilon)$, is a stationary random variable of order 2 on the interval $(0, L]$. Thus $X_i(\epsilon)$ is a concentration value derived by dividing the measure $\mu_i(\epsilon)$ by its linear cell size ϵ. Its mean $E\{X_i(\epsilon)\} = \xi$ is assumed to be independent of ϵ, and the covariance for lag h satisfies $\text{cov}(h) = E\{[X_i(\epsilon) - \xi][X_{i+h}(\epsilon) - \xi]\}$. In De Wijs's example (see later), $X_i(\epsilon)$ is represented by zinc assay values for 118 channel samples obtained at 2.00-m intervals along a drift in the Pulacayo sphalerite-quartz vein. In order to study the frequency distribution and spatial characteristics of $X_i(\epsilon)$, a series of samples can be collected. For simplification we assume that these samples are located regularly within $(0, L]$ in that adjoining samples have equal size. Consequently, the interval $(0, L]$ is subdivided into $N(\epsilon) = L/\epsilon$ cells, each of size ϵ. The average value $X_j(k\epsilon)$ of a larger cell with size $k\epsilon$ can be expressed as

$$X_j(k\epsilon) = \frac{1}{k} \sum_{i=(j-1)k+1}^{jk} X_i(\epsilon) \tag{4}$$

with $j = 1, \ldots, N_k$, where $N(\epsilon)/k - 1 < N_k \leq N(\epsilon)/k$ is the total number of cells of size $k\epsilon$.

Variance (σ^2), covariance (cov), auto-correlation (ρ), and semivariogram

(γ) of the random variable $X_i(\epsilon)$ can be estimated using

$$\sigma^2(\epsilon) = \frac{1}{N(\epsilon)} \sum_{i=1}^{N(\epsilon)} [X_i(\epsilon) - \xi(\epsilon)]^2 \tag{5}$$

$$\text{cov}\ (h) = \sigma_h(\epsilon) = \frac{1}{N(\epsilon) - h} \sum_{i=1}^{N(\epsilon)-h} [X_i(\epsilon) - \xi(\epsilon)][X_{i+h}(\epsilon) - \xi(\epsilon)] \tag{6}$$

$$\rho_h(\epsilon) = \frac{\text{cov}\ (h)}{\sigma^2(\epsilon)} \tag{7}$$

$$\gamma_h(\epsilon) = \frac{1}{2[N(\epsilon) - h]} \sum_{i=1}^{N(\epsilon)-h} [X_i(\epsilon) - X_{i+h}(\epsilon)]^2 \tag{8}$$

where $\xi(\epsilon)$ represents the average value of $X_i(\epsilon)$ in $(0, L]$ with $i = 1, \ldots, N(\epsilon)$, and h is lag. Suppose, as before, that the measure $\mu_j(\epsilon)$ either has the multifractal property and satisfies Equations (1) to (3), or that its first- and second-order moments have fractal properties so that Equation (2) holds true for $q = 1$ and $q = 2$ if modeling is restricted to the spatial statistics of Equations (5) to (8). Setting $q = 1$ in Equations (1) and (2) gives for the first moment

$$\xi(\epsilon) = \frac{1}{N(\epsilon)} \sum_{j=1}^{N(\epsilon)} X_j(\epsilon) = \frac{1}{L} \sum_{j=1}^{N(\epsilon)} \mu_j(\epsilon) = c_1 \epsilon^{\tau(1)} = \xi \tag{9}$$

where $c_1 = \xi$ is constant, because the total quantity ($= \xi L$) must be preserved implying $\tau(1) = 0$ (principle of conservation of total mass). Setting $q = 2$ in Equations (1) and (2), gives the noncentered second-order moment $\xi_2(\epsilon)$ with

$$\xi_2(\epsilon) = \frac{1}{N(\epsilon)} \sum_{j=1}^{N(\epsilon)} [X_j(\epsilon)]^2 = \frac{1}{\epsilon L} \sum_{j=1}^{N(\epsilon)} [\mu_j(\epsilon)]^2 = c_2 \epsilon^{\tau(2)-1} \tag{10}$$

where c_2 is another constant. From Equations (9) and (10), it follows that

$$\sigma^2(\epsilon) = c_2 \epsilon^{\tau(2)-1} - \xi^2 \tag{11}$$

Consequently,

$$\sigma^2(k\epsilon) = \sigma^2 \left[\frac{1}{k} \sum_{i=(j-1)k+1}^{jk} X_i(\epsilon) \right] = c_2 (k\epsilon)^{\tau(2)-1} - \xi^2 \tag{12}$$

Combining Equation (12) with the following equality (e.g., see Bartlett, 1966, p. 284)

$$\sigma^2 \left[\frac{1}{k} \sum_{i=1}^{k} X_i(\epsilon) \right] = \frac{\sigma^2(\epsilon)}{k} \left[1 + 2 \sum_{s=1}^{k-1} \left(1 - \frac{s}{k} \right) \rho_s(\epsilon) \right] \tag{13}$$

it is derived that

$$k^2[c_2(k\epsilon)^{\tau(2)-1} - \xi^2] = \sigma^2(\epsilon)\left[k + 2\sum_{s=1}^{k-1}(k-s)\rho_s(\epsilon)\right] \tag{14}$$

and, by elementary methods,

$$\rho_k(\epsilon) = \frac{c_2\epsilon^{\tau(2)-1}}{2\sigma^2(\epsilon)}[(k+1)^{\tau(2)+1} - 2k^{\tau(2)+1} + (k-1)^{\tau(2)+1}] - \frac{\xi^2}{\sigma^2(\epsilon)} \tag{15}$$

For small ϵ or if $\xi \ll \sigma(\epsilon)$, the last term in Equation (15) can be neglected, and

$$\rho_k(\epsilon) \simeq \rho_k = \tfrac{1}{2}[(k+1)^{\tau(2)+1} - 2k^{\tau(2)+1} + (k-1)^{\tau(2)+1}] \tag{16}$$

Similarly,

$$\mathrm{cov}_k(\epsilon) = \tfrac{1}{2}c_2\epsilon^{\tau(2)-1}[(k+1)^{\tau(2)+1} - 2k^{\tau(2)+1} + (k-1)^{\tau(2)+1}] - \xi^2 \tag{17}$$

and

$$\gamma_k(\epsilon) = c_2\epsilon^{\tau(2)-1}[1 - \tfrac{1}{2}\{(k+1)^{\tau(2)+1} - 2k^{\tau(2)+1} + (k-1)^{\tau(2)+1}\}] \tag{18}$$

The semivariogram has sill $\gamma_\infty(\epsilon) = c_2\epsilon^{\tau(2)-1}$ which depends on the value of cell size ϵ. As cell size decreases to zero, the sill increases infinitely. The covariance also depends on cell size but the autocorrelation function is relatively independent of it. Replacement of the second-order difference in Equation (16) by the second derivative yields

$$\rho_k(\epsilon) \simeq \tfrac{1}{2}\{\tau(2) + 1\}\tau(2)k^{\tau(2)-1} \tag{19}$$

Likewise, Equations (17) and (18) can be approximated by

$$\mathrm{cov}_k(\epsilon) \simeq \tfrac{1}{2}c_2\epsilon^{\tau(2)-1}\{\tau(2) + 1\}\tau(2)k^{\tau(2)-1} - \xi^2 \tag{20}$$

and

$$\gamma_k(\epsilon) \simeq c_2\epsilon^{\tau(2)-1}[1 - \tfrac{1}{2}\{\tau(2) + 1)\}\tau(2)k^{\tau(2)-1}] \tag{21}$$

Hence, provided that $\tau(2)$ is only slightly less than 1,

$$\gamma_k(\epsilon) \simeq -c_2\epsilon^{\tau(2)-1}\log[\tfrac{1}{2}\{(k+1)^{\tau(2)+1} - 2k^{\tau(2)+1} + (k-1)^{\tau(2)+1}\}] \tag{22}$$

or

$$\gamma_k(\epsilon) \simeq -c_2\epsilon^{\tau(2)-1}\log[\tfrac{1}{2}\{\tau(2) + 1\}\tau(2)k^{\tau(2)-1}] \tag{23}$$

This last expression shows that the semivariogram may be approximately linear in log k.

Anyone of the functions Equations (15) to (23) can be used for modeling a one-dimensional series of measurements. If the underlying spatial structure is multifractal, the best results are obtained by Equations (15), (17), and (18). The relatively simple power-law relations of Equations (19) to (21) then provide less satisfactory results unless the series is long. On the other hand, Equation (23) can give good results, even for series consisting of relatively few measurements (see later).

COMPARISON TO OTHER MODELS

The purpose of this section is to review briefly several earlier power-law type equations for spatial statistical analysis which are not identical to but closely resemble those derived in the previous section. A geostatistical (De Wijsian) model resulting in a semivariogram similar to Equation (23) was introduced originally by Matheron (1962). The equations for spatial statistics derived in the previous section also can be approximately by empirical equations proposed by Fairfield-Smith (1938) and Yaglom (1966). Of these authors, Fairfield-Smith used an equation similar to Equation (11) (see later). Before the development of multifractal theory, Yaglom (1966) introduced a model with power-law type second-order mass exponent similar to Equation (10). From this he derived expressions similar to Equations (11) and (20). Mandelbrot (1983), Mandelbrot and Van Ness (1968), Taqqu (1988), and Rose (1983; 1992) used fractal modeling to derive equations for spatial statistics as will be discussed briefly in the next three subsections.

Mandelbrot's Fractional Brownian Motion Model

Suppose that η_i represents a random variable with zero mean for length of step (labeled i) of a particle engaged in fractional Brownian motion, moving forward or backward along an axis (cf. Feder, 1988, p. 166). After j successive steps η_i, the position ζ_j of this particle is

$$\zeta_j = \sum_{i=1}^{j} \eta_i \tag{24}$$

with semivariogram

$$\tfrac{1}{2} E[\zeta_j - \zeta_{j+k}]^2 \propto k^{2H} \tag{25}$$

where H is the Hurst exponent with $0 \leq H \leq 1$; $H = 1/2$ corresponds to the special situation of Brownian motion with independent increments. As discussed by Mandelbrot (1983), ζ_j can be interpreted as the elevation at a point labeled

j along a sampling line across a fractal landscape with fractal dimension $3 - H$. The fractal dimension D for any profile across the landscape equals $D = 2 - H$.

As shown originally by Mandelbrot and Van Ness (1968), the autocorrelation ρ_k between the elevations ζ_j and ζ_{j+k} of two points on a fractal landscape satisfies an expression similar to Equation (16) with $\tau(2) + 1 = 2H$. Consequently, Equation (25) is equivalent to

$$E[\zeta_j - \zeta_{j+k}]^2 = E\left[\sum_{i=j+1}^{j+k} \eta_i\right]^2 = c_2 \epsilon^{\tau(2)-1} k^{\tau(2)+1} \tag{26}$$

as follows from Equation (10), and $H = 1/2\{\tau(2) + 1\}$. Fractional Brownian motion is persistent if $1/2 < H \leq 1$ or $0 < \tau(2) \leq 1$, and antipersistent if $0 \leq H < 1/2$ or $-1 \leq \tau(2) < 0$. The limiting situations $\tau(2) = 1$ and $\tau(2) = -1$ result in $\rho_k(\epsilon) =$ constant, $k = 1, 2, \ldots$.

Taqqu's Model

A power-law type of variance

$$\sigma^2(X_k) \propto k^{2H} \tag{27}$$

for self-similar processes X_k with stationary increments satisfying Equation (16) was proposed by Taqqu (1988). From Equation (12), after multiplication by k^2, it follows that

$$\sigma^2[X(k\epsilon)] = \sigma^2\left[\sum_{i=1}^{k} X_i(\epsilon)\right] = c_2 k^2 (k\epsilon)^{\tau(2)-1} - k^2\xi^2 \tag{28}$$

If $\xi = 0$, this would become similar to Equation (27). In practical applications, the condition $\xi = 0$ could be forced to be satisfied approximately by subtracting an estimate of the mean from the observed values. However, Equations (10) and (11) then would become identical. This, in turn, would imply that the multifractal model would not be valid for $q = 2$.

Rose's Model

In general, the autocorrelation of average values of adjoining cells of size $k\epsilon$ satisfies

$$\rho_1(k\epsilon) = \frac{2\sigma^2[X(2k\epsilon)]}{\sigma^2[X(k\epsilon)]} - 1 \tag{29}$$

In combination with Equation (12) this yields

$$\log\left[\{1 + \rho_1(k\epsilon)\}/2\right] = [1 - 2^{\tau(2)-1}]\frac{c_2(k\epsilon)^{\tau(2)-1}}{\xi^2} \tag{30}$$

An empirical variance-size relation

$$\sigma^2[X(k\epsilon)] = k^{-b}\sigma^2[X(\epsilon)] \tag{31}$$

where b is a constant was proposed originally by Fairfield-Smith (1938). Setting $b = 1 - \tau(2)$, Equation (31) follows from Equation (16) if $\xi = 0$. Keeping $\xi > 0$, Rose (1983, 1992) derived Equation (31) as well as Equation (16) from a postulate on similarity of autocorrelation which can be expressed as

$$\rho_1(\epsilon_1) = \rho_1(\epsilon_2) \tag{32}$$

where ϵ_1 and ϵ_2 are any two different small segments, for example, $\epsilon_1 = \epsilon$ and $\epsilon_2 = k\epsilon$. However, according to Equation (30) $\rho_1(k\epsilon)$ depends on k. It also would follow from Equation (32) that

$$\rho_1(k\epsilon) = 2^{\tau(2)} - 1 \tag{33}$$

If $\xi > 0$, Equation (33) is approximately equal to Equation (30) only if $\tau(2)$ is close to 1.

It may be concluded that Rose's model is likely to give results which are similar to those produced by the multifractal model. However, there will be differences which can become large depending on the magnitude of $1 - \tau(2)$. Most of the differences in results of spatial analysis between the multifractal model and the other models based on fractal modeling discussed in this section are related to the fact that the last term of Equation (17) satisfies $\xi^2 = 0$ for the other models.

EXAMPLE: APPLICATION TO DE WIJS'S ZINC VALUES

De Wijs (1951) studied assay values from the Pulacayo sphalerite-quartz vein in Bolivia. These data will be used for example in the remainder of this paper. Along a drift 118 channel samples had been collected at 2.00 meter intervals (see Fig. 1A). The massive sulphide vein was on average about 0.50-m wide but all samples were cut over the anticipated stoping width of 1.30 m. These channel samples provide unbiased estimates of the zinc concentration in 2-m-long blocks measured along the vein in the direction of the vein. It is noted, however, that these average zinc values for 2-m-long blocks would have a frequency distribution that is narrower than the one for the channel samples shown in Figure 1B (cf. Agterberg, 1994).

The Multifractal Spectrum of the Zinc Values

A measure $\mu_i(\epsilon) = \epsilon X_i(\epsilon)$, $i = 1, \ldots, 118$, was defined as in Equation (4) with $X_i(\epsilon)$ representing the concentration of zinc per unit length. Cell sizes ranging from 2 m to 30 m (total length is 234 m) were used. Some results of

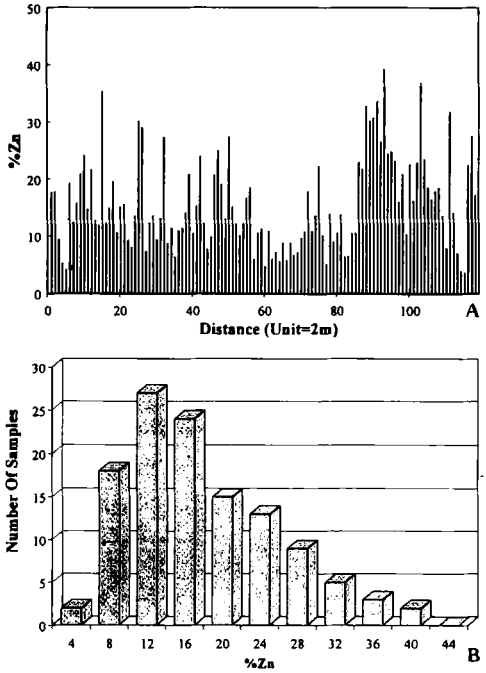

Figure 1. A, Zinc concentration values in 2-m segments (data from De Wijs, 1951); B, Histogram of zinc values.

estimating the partition function with q ranging from -34 to 34 are shown in Figure 2A using log-log paper. For each value of q a straightline was fitted by linear regression of log $\chi(\epsilon)$ on log ϵ (ordinary least squares). The slopes, $\hat{\tau}(q)$, of all fitted straightlines with $q = -35, -34, \ldots, -1, 0, 1, \ldots 50$ are shown in Figure 2B. These results include $\hat{\tau}(0) = -0.976 \pm 0.011$ where the uncertainty is expressed using the standard deviation ($\pm s$). According to Equation (3) the box-counting dimension is estimated to be 0.976 ± 0.011. It is noted that the slope for $q = 1$ is approximately equal to zero as expected (principle of conservation of total mass). Figure 3 shows the best-fitting line for $q = 2$ which passes nearly exactly through the data points. Its slope being $\hat{\tau}(2) = 0.979 \pm 0.019$ provides an estimate of the second-order mass exponent and will be used extensively in the next section.

Successive estimates of $\hat{\tau}(q)$ were connected by straightline segments (Fig. 2B) which, together, form an approximately differentiable curve. Values of the singularity α (see Fig. 2C) were estimated by applying the central difference technique to successive sets of three values of $\hat{\tau}(q)$. The multifractal spectrum

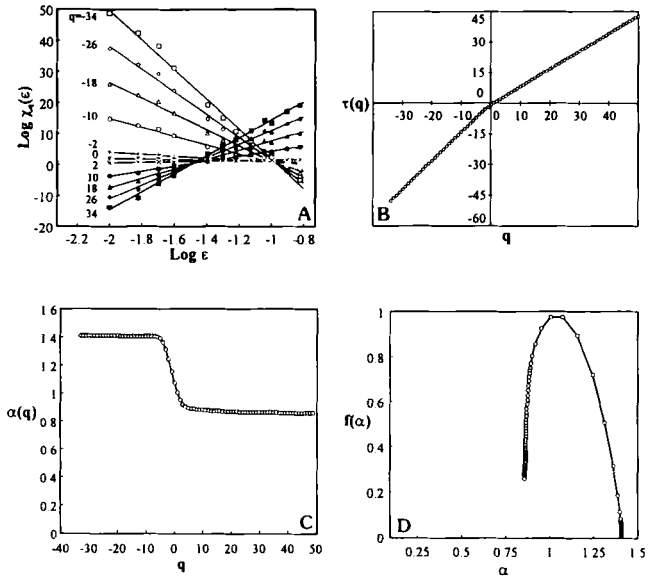

Figure 2. Results of multifractal analysis applied to zinc concentration values in Figure 1. A, Log-log plot for relationship between $\chi_q(\epsilon)$ and ϵ; straightlines obtained by method of least squares (LS). B, Estimates of $\tau(q)$ include slopes of straightlines in A. C, Singularity α estimated from B by central difference method, and D, multifractal spectrum $f(\alpha)$. Smallest cell size $\epsilon = 1/100$ corresponds to 2 m; logarithmic scales have base 10.

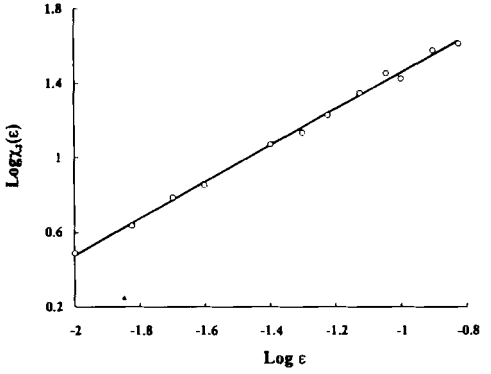

Figure 3. Log-log plot for relationship between $\chi_2(\epsilon)$ and ϵ.

$f(\alpha)$ (Fig. 2D) was derived from the values shown in Figure 2B and 2C by Equation (3).

The results of Figure 2 show that the zinc concentration values are multifractal instead of fractal. A fractal model would have resulted in a single straightline in Figure 2B, a horizontal line in Figure 2C, and a vertial spike in Figure 2D, respectively. The straightlines in Figure 2A would have had interrelated slopes $\tau(q)/(q-1) = \tau(p)/(p-1)$ for any pair of values of $q \neq p$ in a simple fractal model, for example, $\tau(12) = -\tau - 10$ when $q = 12$ and $p = -10$. Linear regression for these values gave the estimates $\hat{\tau}(12) = 9.8709 \pm 0.2192$ and $\hat{\tau}(-10) = -14.1243 \pm 0.4267$. The absolute value of the difference of these slopes is 4.2534 ± 0.4797 which is different significantly from 0. This clearly shows that the underlying model is multifractal instead of fractal.

Relation to Binomial Multiplicative Cascade Model

The so-called binomial multiplicative cascade model in [1] is the simplest multifractal self-similar model in existence. It has been discussed by several authors including Feder (1988) and Evertsz and Mandelbrot (1992). It is introduced here for the following two reasons: (a) it help us to understand the nature of multifractal models and how they can be constructed, and (b) it provides a possible explanation for the results shown in Figure 2.

A stochastic version of the binomial model is as follows (Meneveau and Sreenivasan, 1987; Agterberg, 1994). At the first stage ($k = 1$) in a process consisting of k stages, the interval $(0, L]$ with measure ξL is subdivided into two equal intervals: (a) $(0, L/2]$ with measure $(1 + B)\xi L$, and (b) $(L/2, L]$ with $(1 - B)\xi L$, where B is a random variable with $\text{pr}(B = d) = \text{pr}(B = -d) = 1/2$ $(d > 0)$. At stage 2 these two intervals are halved again with new measures for the halves defined in the same way as at stage 1. The process is repeated at stages $k = 3, 4, \ldots$. At stage k the ith subinterval with value $X_i(\epsilon)$ has size $\epsilon = L/2^k$, and $E\{X_i(\epsilon)\} = \xi$. The frequency distribution of $X_i(\epsilon)$ is logbinomial, tending to become lognormal in the center as $\epsilon \to 0$ and, depending on the direction of ordering, Pareto in both tails.

Defining a new constant $m = (1 + d)/2$, it can be shown (Evertsz and Mandelbrot, 1992, p. 941) that, as $k \to \infty$,

$$\tau(q) = -\log_2 [m^q + (1 - m)^q] \tag{34}$$

with corresponding expressions for $\alpha(q)$ and $f(\alpha)$ immediately following from Equation (3). The resulting multifractal spectrum has its maximum at the point where $f(\alpha) = 1$ for $\alpha = \alpha(0)$. It resembles a parabola in the center but is truncated at the bottom because $f(\alpha) \geq 0$. The smallest and largest values of α are $\alpha_{\min} = -\log_2 m$ and $\alpha_{\max} = -\log_2 (1 - m)$, respectively.

The binomial model would predict exact symmetry for the curve of Figure

2D and this condition obviously is not satisfied in practice. There are two reasons why the binomial model could be valid because of bias in the pattern of Figure 2D: (a) although, individually, they are unbiased, the original zinc assay values have a variability that overestimates the (unknown) true variability of the larger 2-m-long blocks they represent, and (b) the method used to arrive at the multifractal spectrum of Figure 2D is subject to (unknown) propagation of sampling errors, especially those related to the differentiation of $\tau(q)$. These difficulties can be resolved partially by arguing as follows.

The estimate $\hat{\tau}(2) = 0.979 \pm 0.019$ derived in Figure 3 probably is relatively good as suggested by its relatively small standard deviation. Its substitution into Equation (34) gives $-\log_2 \{\hat{m}^2 + (1 - \hat{m})^2\} = 0.979$, from which it follows that $\hat{m} = 0.560$ with $\alpha_{\min} = 0.84$. This is in agreement with the smallest values of α suggested by the curves in Figures 2C and 2D. In the next section it will be seen that $\hat{\tau}(2) = 0.979 \pm 0.019$ also gives good results for spatial statistics.

The increase in variability resulting from channel sampling (see before), is likely to have resulted in increased absolute values of the slopes in Figures 2A and 2B, including $\hat{\tau}(2) = 0.979$. Propagation of this bias would lead to a true value of $\alpha_{\min}$ greater than 0.84. On the other hand, the straightlines used to estimate $\tau(q)$ for negative values of q (e.g., $q = -10$) show a relatively good fit in Figure 2A. Because of Equation (3) this would imply that the right tail of the curve in Figure 2D provides a good estimate. It can be shown that this, in turn, would indicate that the true value of $\alpha_{\min}$ is less than 0.84 under the binomial assumption. Because of these sources of uncertainty, it can be concluded only that the spatial structure underlying Figure 1 probably is multifractal with properties equal or close to those of the binomial multiplicative cascade model.

The preceding estimate of $\hat{m} = 0.56$, which was based on $\hat{\tau}(2) = 0.979$, results in $\hat{d} = 0.120$. If the underlying model would be binomial with this parameter, halving any sufficiently long interval within the vein would give half-intervals with the property that the half-interval with the greater density has density of zinc values approximately $(1 + \hat{d} =)\ 1.12\times$ greater than before the subdivision. This is equivalent to stating that, for two adjoining samples, the value of the sample with the greater zinc concentration is approximately 1.27 times as large as the value of the other sample. These rules are only approximately valid (cf. De Wijs, 1951).

Autocorrelation and Semivariogram Functions

Covariance, autocorrelation, and semivariogram values for successive lags were estimated from the data by Equations (6) to (8) with the unit of lag set equal to 2 m. The estimate $\hat{\tau}(2) = 0.979$ resulting from Figure 3 was used as

a coefficient for comparison with fitted curves satisfying Equations (15), (17), and (18). The other coefficients in these equations were estimated by ordinary least squares. For $k \leq 13$, this gave

$$\hat{\rho}(k) = 4.37[(k+1)^{1.979} - 2k^{1.979} + (k-1)^{1.979}] - 8.00$$

$$\hat{\sigma}(k) = 277.65[(k+1)^{1.979} - 2k^{1.979} + (k-1)^{1.979}] - 5.8087$$

$$\hat{\gamma}(k) = 391.49 - 180.38[(k+1)^{1.979} - 2k^{1.979} + (k-1)^{1.979}] \quad (35)$$

This result is shown graphically in Figure 4 for the covariance function, using arithmetic as well as logarithmic scales. Similar results for the semivariogram are shown in Figure 5 after increasing the maximum lag. The curve displayed in different ways in Figure 5A and 5B satisfies Equation (18) with $\hat{\tau}(2) = 0.979$. The other coefficients in this equation were estimated by least squares. Figure 5C shows results for the logarithmic semivariogram model of Equation (23) with

$$\hat{\gamma}(k) = 36.9 + 22.31 \log(k) \quad (36)$$

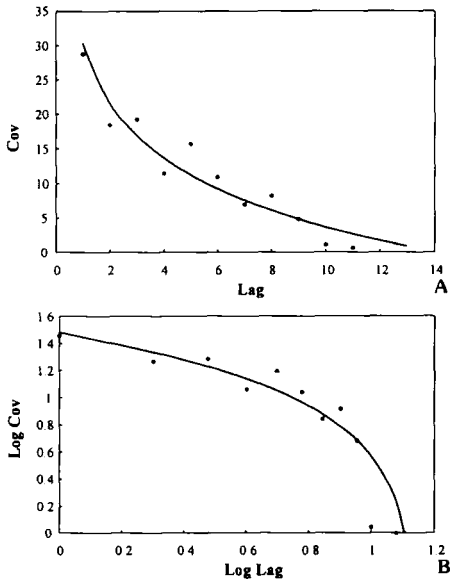

Figure 4. Estimated covariance values and fitted curves satisfying Equation (17) for zinc concentration values (distance $k \leq 13$). A, solid line obtained by linear regression after setting $\hat{\tau}(2) = 0.979$. B, Log-log plot of A. Zinc values measured as percentages (see Fig. 1). Unit of lag is 2 m; logarithms base 10.

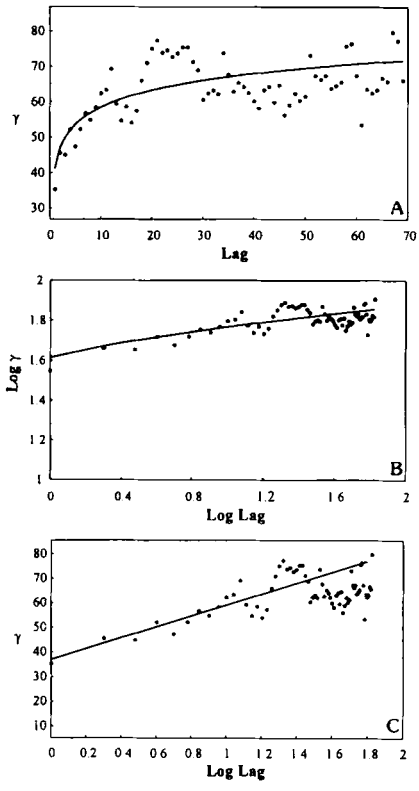

Figure 5. Estimates of semivariogram γ_k. A, Solid line satisfying Equation (18) obtained by linear regression after setting $\hat{\tau}(2) = 0.979$. B, Log-log plot of A. C, Logarithmic model of Equation (23). Units along axes as in Figure 4.

where both coefficients were obtained by ordinary least squares. The result shown in Figure 5C is comparable to results of models previously applied by Matheron (1962, p. 180) and Agterberg (1994, p. 226). It may be concluded that the equations resulting from the multifractal model with $\hat{\tau}(2) = 0.979$ also can be used for modeling the spatial covariance and semivariogram function in this example.

CONCLUDING REMARKS

In general, the multifractal model provides more information about measurements on spatial objects than ordinary fractal models. The mass exponent function $\tau(q)$ is useful for characterizing the underlying structure of the measurements with $-\tau(0)$ corresponding to the largest fractal dimension (= box-counting dimension of the support) and $\tau(2)$ determing the spatial covariance of

continuous random variables. The most useful second-order functions including Equations (15), (17), and (18) are nonlinear but can be fitted to data by linear least squares if a good estimate of $\tau(2)$ is available. Multifractal modeling also can be applied to spatial point processes (Cheng and Agterberg, 1995).

The approach was illustrated by an example (De Wijs's zinc values), showing (a) validity of the multifractal model in the situation, and (b) usefulness of the newly derived second-order functions for modeling spatial variability. In this case-history study, the box-counting dimension ($\approx$ 1) of the support is approximately Euclidian. The estimated first-order mass exponent $\tau(1)$ is close to zero as expected.

ACKNOWLEDGMENTS

This paper is based on Cheng's (1994) Ph.D. dissertation at the University of Ottawa. Thanks are due to Drs. G. F. Bonham-Carter, Geological Survey of Canada, Ottawa, A. D. Fowler, University of Ottawa, I. Lerche, University of South Carolina, Columbia, and G. Ranalli, Carleton University, Ottawa, for helpful comments. Geological Survey of Canada Contribution No. 20294.

REFERENCES

Agterberg, F. P., 1994, Fractals, multifractals, and change of support, *in* Dimitrakopoulus, R., ed., Geostatistics for the next century: Kluwer, Dordrecht, p. 223–234.

Agterberg, F. P., Cheng, Q., and Wright, D. F., 1993, Fractal modeling of mineral deposits, *in* Elbrond, J., and Tang, X., eds., Application of computers and operations research in the mineral industry: Proc. 24th APCOM Symposium, v. 1, Can. Inst. Mining, Metallurgy and Petroleum Eng. (Montreal), p. 43–53.

Bartlett, M. S., 1966, An introduction to stochastic processes (2nd ed.): Cambridge Univ. Press, Cambridge, 362 p.

Billingsley, P., 1986, Probability and measure (2nd ed.): John Wiley & Sons, New York, 622 p.

Cheng, Q., 1994, Multifractal modeling and spatial analysis with GIS: Gold potential estimation in the Mitchell-Sulphurets area, northwestern British Columbia: unpubl. doctoral dissertation, Univ. Ottawa, Ottawa, 268 p.

Cheng, Q., and Agterberg, F. P., 1995, Multifractal modeling and spatial point processes: Math. Geology, v. 27, no. 7, p. 831–845.

Cheng, Q., Agterberg, F. P., and Ballantyne, S. B., 1994, The separation of geochemical anomalies from background by fractal methods: Jour. Geochemical Exploration, v. 51, no. 2, p. 109–130.

Csörgö, M., and Révész, P., 1981, Strong approximations in probability and statistics: Academic Press, New York, 284 p.

De Wijs, H. J., 1951, Statistics of ore distribution: Geologie en Mijnbouw, v. 13, no. 8, p. 365–375.

Evertsz, C. J. G., and Mandelbrot, B. B., 1992, Multifractal measures, *in* Peitgen, H.-O., Jürgens, H., and Saupe, D., eds., Chaos and fractals: Springer Verlag, New York, p. 922–953.

Fairfield-Smith, H., 1938, An empirical law describing heterogeneity in the yields of agricultural crops: Jour. Agricultural Sci., v. 28, no. 1, p. 1–23.

Feder, J., 1988, Fractals: Plenum, New York, 283 p.

Hentschel, H. G. E., and Procaccia, I., 1983, The infinite number of generalized dimensions of fractals and strange attractors: Physica, v. 8, pt. D, p. 435–444.

Mandelbrot, B. B., 1983, The fractal geometry of nature (updated and augmented edition): W.H. Freeman and Company, New York, 468 p.

Mandelbrot, B. B., and Evertsz, C. J. G., 1991, Exactly self-similar left-sided multifractals, *in* Bunde, A., and Havlin, S., eds., Fractals and disordered systems: Springer Verlag, Heidelberg, p. 323-344.

Mandelbrot, B. B., and Van Ness, J. W., 1968, Fractional brownian motions, fractional noises and applications: SIAM Review, v. 10, no. 4, p. 422–437.

Matheron, G., 1962, Traité de Géostatistique Appliquée. Mém. Bur. Rech. Géol. Minières, v. 14, p. 1-333.

Meneveau, C., and Sreenivasan, K. R., 1987, Simple multifractal cascade model for fully developed turbulence: Phys. Review Letters, v. 59, no. 13, p. 1424-1427.

Rose, C. D., 1983, Variances in sampling streams of coal: Jour. Testing and Evaluation, v. 11, p. 320–330.

Rose, C. D., 1992, A fractal model for sampling coal, ores, and other natural populations: Jour. Coal Quality, v. 11, no. 1-2, p. 6–13.

Stanley, H. E., and Meakin, P., 1988, Multifractal phenomena in physics and chemistry: Nature, v. 335, no. 6189, p. 405–409.

Taqqu, M. S., 1988, *in* Kotz, S., and Johnson, N., eds., Self-similar processes: Ency. of Stat. Sci., v. 8: John Wiley & Sons, New York, p. 352–357.

Yaglom, A. M., 1966, The influence of fluctuations in energy dissipation on the shape of turbulence characteristics in the inertial interval: Soviet Physics-Doklady, v. 11, p. 26–29.